

A Decomposition-Based Hybrid Ensemble CNN Framework for Improving Cross-Subject EEG Decoding Performance

Ruilin Li, Ruobin Gao *Member, IEEE*, P. N. Suganthan, *Fellow, IEEE*

Abstract— Electroencephalogram (EEG) signals are complex, non-linear, and non-stationary in nature. Several decomposition methods have been applied to minimize the signal complexity and improve the EEG decoding performance. However, previous studies mainly exploited the hand-engineering features, limiting the information learned in EEG decoding. Therefore, extracting additional primary features from different disassembled components to improve the EEG-based recognition performance remains challenging. On the other hand, attempts have been made to use a single model to learn the hand-engineering features. Less work has been done to improve the generalization ability through ensemble learning. In this work, we propose a novel decomposition-based hybrid ensemble convolutional neural network (CNN) framework to enhance the capability of decoding EEG signals. CNNs, in particular, automatically learn the primary features from raw disassembled components but not handcraft features. Furthermore, to comprehensively exploit the diverse information from decomposed components, we employ two ensemble modes that integrate all CNNs outputs. The first option is to fuse the obtained score before the Softmax layer and execute back-propagation on the entire ensemble network, whereas the other is to fuse the probability output of the Softmax layer. Moreover, a component-specific batch normalization (CSBN) layer is employed to reduce subject variability. Against the challenging cross-subject driver fatigue-related situation awareness (SA) recognition task, eight models are proposed under the framework, which all showed superior performance than the strong baselines. The performance of different decomposition methods and ensemble modes were further compared. Results indicated that discrete wavelet transform (DWT)-based ensemble CNN achieves the best 82.11% among the proposed models. Our framework can be simply extended to any CNN architecture and applied in any EEG-related sectors, opening the possibility of extracting more preliminary information from complex EEG data.

Index Terms— Electroencephalogram (EEG); Signal Decomposition; Ensemble Learning; Convolutional Neural Network (CNN); Cross-Subject Situation Awareness (SA) Recognition

I. INTRODUCTION

Decoding electroencephalogram (EEG) for human states recognition is objective and in real-time for practical applications. Therefore, it is becoming increasingly popular for use in operator monitoring, training and warning systems [1]. However, due to its complexity and non-stationarity, EEG decoding performance in cross-subject recognition tasks is limited [2]. In this work, we consider the problems in the direction of reducing the complexity to different components and performing simpler learning tasks on them such that more primary information can be captured.

Corresponding author: P. N. Suganthan

Ruilin Li is with Cognitive Human-Machine Interaction Lab, Fraunhofer Singapore, Singapore 639798, and also with School of Electrical and Electronic Engineering, Nanyang Technological University, Singapore (e-mail: RUILIN001@e.ntu.edu.sg).

Ruobin, Gao is with School of Civil and Environmental Engineering, Nanyang Technological University, Singapore (e-mail: GAOR0009@e.ntu.edu.sg).

P. N. Suganthan is with School of Electrical and Electronic Engineering, Nanyang Technological University, Singapore (e-mail: EPNSugan@ntu.edu.sg).

Various decomposition methods have been applied to EEG signals to improve the decoding performance [3]. There are mainly two categories to exploit the disassembled components. The first way is to perform hand-engineering feature extraction based on the prior knowledge of the signal, followed by classifier training. Anuragi *et al.* [4] computed entropy-based features from Euclidean distances of 3D phase-space representation (PSR) of components decomposed by empirical wavelet transform (EWT). After feature extraction based on the Kruskal-Wallis statistical test, ensemble machine learning classifiers are performed to recognize Epileptic-seizure states. Sairamya *et al.* [5] used relaxed local neighbor difference pattern (RLNDiP) features from the time-frequency domain, consisting of five brain rhythms obtained by discrete wavelet transform (DWT). Artificial neural networks (ANN) were employed for the automatic diagnosis of Schizophrenia. Gu *et al.* [6] exploited non-negative matrix factorization (NMF) and empirical mode decomposition (EMD) to decompose the EEG signal into a set of intrinsic mode functions (IMFs). Statistical features were extracted from the de-noised components and inputted to classifiers such as support vector machine (SVM), etc. PrakashYadav *et al.* [7] applied variational mode decomposition (VMD) to decompose EEG signal of seizure into 14 IMFs. Normalized energy, fractal dimension, number of peaks, and prominence parameters were employed as extracted features. A Bayesian regularized shallow neural network was proposed to perform the classification task. Interestingly, Sadiq *et al.* [8] considered decomposed component as a feature vector and further applied methods like neighborhood component analysis (NCA) to reduce the huge dimension of the feature matrix. Although this study tried to exploit raw data, an information loss problem existed. On the other hand, decomposition methods were exploited to reduce the noise of the signals. Feature selection was performed on each component to reduce the noise more meticulously. For instance, Aliyu *et al.* [9] used correlation and *p*-value analysis to select optimal features computed on the decomposed components by DWT. Unlike the component-wise selection, some other researchers directly selected the most effective components using some criteria and dropped the rest. Wang *et al.* [10] exploited sample entropy of each IMF that VMD obtains to select the maximum one to train the classifier further. In conclusion, decomposition can obtain simpler patterns, which makes the signal easier to analyze. However, less attention has been paid to learning patterns directly on raw components data, which has the potential to extract the primary information for the recognized states more precisely. In addition, although some feature selection methods can help reduce the noise, the problem of information loss exists simultaneously. How to properly capture useful patterns and eliminate the redundant information from different components is a research problem.

It has made an outstanding performance to exploit deep convolutional neural networks (CNNs) to decode EEG signals in an end-to-end fashion. Schirrmeister *et al.* [11] were the first to comprehensively study the design and training of CNN by using raw EEG data. A shallow and deep CNN architecture was designed, which showed better performance than FBSCP on motor imagery classification. CNNs with different architectures have been tried for various EEG-based recognition tasks. For instance, CNNs with the input of spectrogram of EEG were used for mental workload classification

[12] and for motor imagery classification [13]. An adaptive method based on stacked denoising auto-encoders was proposed for mental workload classification as well [14]. However, these models were limited to specific domains. In 2017, Lawhern *et al.* [15] proposed a compact CNN named EEGNet that can be applied on different brain-computer interface (BCI) paradigms and achieved good performance in subject-dependent and subject-independent settings. Moreover, Cui *et al.* [16] proposed an InterpretableCNN which performed spatial and temporal convolution operations, which had been shown the superiority on drowsiness EEG signal decoding and improved the subject-independent recognition accuracy compared with EEGNet. Apart from commonly used 2-dimension CNN, other architectures, such as long-short term memory (LSTM) networks [17], and 3D CNN [18], have presented promising results for corresponding BCI paradigms as well. Previous studies have shown that end-to-end CNN models can improve recognition performance. However, signal complexity and a single model's uncertainty are other constraints for capturing the basic patterns and achieving accurate classifications. Therefore, exploiting CNNs on raw components data is necessary to be investigated. In addition, a single deep neural network (DNN) model used for higher dimension data after decomposition may tend to overfit and suffer from local optima. Compared with a single model, the ensemble model has a more robust capability of learning diverse input data.

To this end, we propose a novel decomposition-based ensemble CNN framework to improve the cross-subject EEG decoding performance. Specifically, decomposition is used to reduce signal complexity. Then, CNNs are employed to learn primary patterns from each raw components signal. Since each component needs to be learned individually and ensemble learning has been proven as a better option for increasing performance [19], the outputs are further integrated with an ensemble architecture. In the framework, two ensemble modes are employed. The first mode is that the score after the fully connected layer is averaged, and all models of this ensemble neural network are trained together, which we call "train CNNs together (TT)." With this setting, the whole model can automatically learn the combination way of outputs. The second one is to directly fuse the outputs of the Softmax layer by average operation, namely "output fusion (OF)." Inputs of decomposed components improve the diversity of the ensemble model, which benefits obtaining better performance. We test our framework on a challenging cross-subject driver fatigue-related situation awareness (SA) recognition task. Results indicated that the proposed models under our framework outperformed the state-of-the-art (SOTA) methods. In particular, DWT-based ensemble CNN with output fusion mode improves performance by roughly 4% when compared to SOTA.

The contributions of this work can be summarized as follows:

- A novel decomposition-based ensemble CNN framework is proposed. CNNs are exploited to extract primary information of individual components, and ensemble architecture is employed to generate the final output. The decomposition techniques enrich the input diversity by disassembling the raw series into components with different characteristics. Then, an individual CNN is utilized to extract primary information from each component. Finally, the ensemble of all CNNs' outputs ensures strong generalizations.
- To the authors' best knowledge, this paper compares different decomposition techniques on the challenging SA recognition task for the first time. The performance of four commonly used decomposition methods is compared, and the comparative results demonstrate that DWT is more suitable for EEG decoding.
- A component-specific batch normalization layer is employed to reduce subject-variability.

- Different types of CNNs for decoding disassembled components are investigated. Signal decomposition boost both shallow and deep CNNs' performance. In particular, deep CNN has better recognition accuracy and is found more suitable for decoding raw components signal.

II. SIGNAL DECOMPOSITION

The nature of the non-periodic and non-stationary EEG signals leads to difficulties in capturing more distinctive features. Thus, signal decomposition algorithms are employed to analyze the signal appropriately in the framework. The algorithms will be introduced in this section.

A. Empirical mode decomposition

The EMD is a purely data-driven method of decomposing a time-domain signal into a set of different mode of oscillations, and a residue. The oscillations mode is defined as the IMF if it satisfies the following two factors [20]:

Factor 1. The number of extrema in the oscillation and the number of zero crossings must equal or differ by at most 1.

Factor 2. The mean of the envelopes defined by the local maxima and the local minima shall equal zero.

The signal decomposed by EMD can be expressed as the sum of a finite number of IMFs and a residual value.

$$x(t) = \sum_{m=1}^k IMF_m(t) + r_k(t), \quad (1)$$

where k is the IMF number and $r_k(t)$ is the final residual value.

The set of IMFs constitutes a complete, adaptive and nearly orthogonal basis for the original signal. The algorithm for the iterative process of Empirical Mode Decomposition is as follows:

- 1) Find all the minima and maxima in $x(t)$.
- 2) Perform cubic spline interpolation of minima to obtain the lower envelope $e_m(t)$ and that of maxima for upper envelope $e_l(t)$.
- 3) Find the mean of the two envelopes using $m(t) = \frac{e_m(t) + e_l(t)}{2}$.
- 4) Subtract the mean from the signal as $d(t) = x(t) - m(t)$.
- 5) Check if $d(t)$ is an IMF or not by applying the factors mentioned above.
- 6) If $d(t)$ is not an IMF, iterate from step (2) to (5) considering input as $d(t)$ to find the IMF.
- 7) If $d(t)$ is an IMF, find the residue $r(t) = x(t) - d(t)$.
- 8) If $r(t)$ has greater than 2 extrema, i.e. one maxima and one minima and a single zero crossing the stopping criterion not satisfied, iterate from step (2) to (5) considering $r(t)$ as input to find the next IMF.
- 9) If $r(t)$ has less than or equal to 2 extrema, i.e. one maxima and one minima and a single zero-crossing the stopping criterion is satisfied and $r(t)$ is the final residue and the EMD process is complete.

The EMD method retains the signal in time domain itself. Each IMF carries information about how the amplitude and frequency of the original signal vary with time. IMFs are composed of a single or a narrow band of frequencies without any overlapping among them. These functions or signals are orthogonal to the original signal. EMD is proved as a beneficial data analysis method, especially for non-stationary, and non-linear EEG signals.

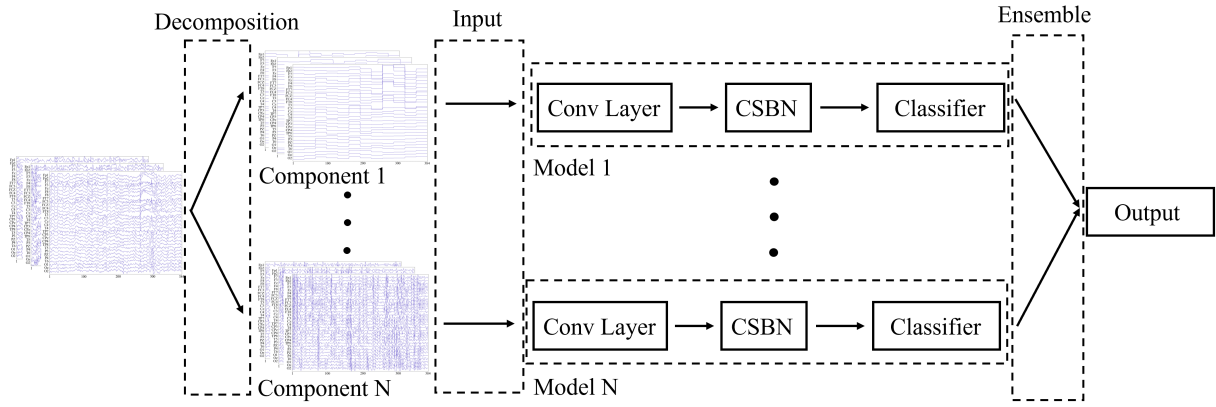


Fig. 1. The structure of the decomposition-based hybrid ensemble CNN framework

B. Discrete wavelet transform and multi-resolution analysis

Fourier transform (FT) has been used for decades to make spectral analysis before wavelet transform. Limited by its inefficiency in local time-frequency representation and unsatisfactory performance to non-stationary signal, wavelet transform has replaced the role of FT and achieved great success in time series analysis.

DWT is calculated as Equation 2,

$$DWTf(j, k) = \langle x(t), \psi_{j,k}(t) \rangle = \int x(t) \psi_{j,k}^*(t) dt, \quad (2)$$

where $\psi_{j,k}(t) = 2^{\frac{j}{2}} \psi(2^j t - k)$, $j, k \in \mathbb{Z}$ is the wavelet function in DWT. In practical forecasting problem, signal $x(t)$ and $\psi_{j,k}(t)$ are both discrete as t is the discrete time index. In reality finite-length times series $x(t) \in L^2(\mathbb{R})$ are all applicable to DWT.

In 1988, [21] first introduces the construction of finite-support orthogonal wavelet named as db wavelet family. For a specific wavelet, there is a pair of scaling function $\phi_{j,k}(t)$ and wavelet function $\psi_{j,k}(t)$ for scale j .

The most important property for scaling function and wavelet function to satisfy the multi-resolution analysis (MRA) is the dilation equation in Equation 3 and 4 based on which MRA is built and it basically indicates that the coarser basis $\phi(t)$ with larger support is a weighted sum of the finer basis $\phi(2t - k)$ with shorter support and $\{h_k, k \in \mathbb{Z}\}$ is the weight.

$$\phi(t) = \sqrt{2} \sum_{k \in \mathbb{Z}} h_k \phi(2t - k) \quad (3)$$

$$\psi(t) = \sqrt{2} \sum_{k \in \mathbb{Z}} g_k \phi(2t - k) \quad (4)$$

As $\{\phi_{j,k}(t), k \in \mathbb{Z}\}$ spans space of scale j (V_j), any function $f_j(t)$ in V_j can be written as a linear combination of the orthogonal base $\{\phi_{j,k}(t), k \in \mathbb{Z}\}$ as

$$f_j(t) = \sum_{k=-\infty}^{\infty} c_j[k] \phi_{j,k}, \quad (5)$$

where $c_j[k]$ is the coefficient of a corresponding basis $\phi_{j,k}$. Based on this representation and Equation 3, 4, the nestedness between space $\{V_j, j \in \mathbb{Z}\}$ can be derived as Equation 6.

$$V_j \subset V_{j+1} \subset \dots V_J, j < J \quad (6)$$

Moreover, the difference(residual) space of two adjacent spaces written as $W_j = V_{j+1} - V_j$ is spanned by wavelet functions

$\psi_{j,k}, (k \in \mathbb{Z})$ due to the orthogonality between $\phi_{j,k}$ and $\psi_{j,k}$ we can effortlessly know that $W_j \perp V_j$.

The scale j of V_j is wavelet-dependent hence various choice of wavelet function (basis) produces different space. However a universal rule of MRA is for scaling function $\phi_{j,k}$, as j increases, its support length diminishes resulting into its resolution being improved and vice versa. An intuitive motivation of applying MRA to time series problem is to decompose a high-resolution signal into the rough trend, the low-frequency cycles and other high frequency components through different corresponding wavelet basis (scaling functions of various scales).

1) Mallat algorithm: In theory, approximation $A_j(t)$ or detail $D_j(t)$ in scale j are calculated through inner product between scaling function $\phi_{j,k}(t)$ or wavelet function $\psi_{j,k}(t)$ and time series $x(t)$ as Equation 7 and 8.

$$A_j(t) = \sum_{k \in \mathbb{Z}} \langle x(t), \phi_{j,k}^*(t) \rangle \phi_{j,k}(t) = \sum_{k \in \mathbb{Z}} c_j[k] \phi_{j,k} \quad (7)$$

$$D_j(t) = \sum_{k \in \mathbb{Z}} \langle x(t), \psi_{j,k}^*(t) \rangle \psi_{j,k}(t) = \sum_{k \in \mathbb{Z}} d_j[k] \psi_{j,k} \quad (8)$$

To get rid of the heavy computation herein, the coefficients $\{c_j[k], k \in \mathbb{Z}\}$ and $\{d_j[k], k \in \mathbb{Z}\}$ are calculated through filtering by leveraging the nestedness of MRA. For the computation of $c_j[k]$ and $d_j[k]$, we can get rid of the expensive sliding inner product by replacing with the much faster convolution and down-sampling as Equation 9.

$$\begin{aligned} c_j[k] &= \sum_i h_{i-2k} \cdot \int f(t) \cdot 2^{(j+1)/2} \phi(2^{j+1}t - i) dt \\ &= \sum_i h_{i-2k} \cdot c_{j+1}[i], \\ d_j[k] &= \sum_i g_{i-2k} \cdot \int f(t) \cdot 2^{(j+1)/2} \psi(2^{j+1}t - i) dt \\ &= \sum_i g_{i-2k} \cdot c_{j+1}[i], \end{aligned} \quad (9)$$

Viewing $\{h_n, n \in \mathbb{Z}\}$ and $\{g_n, n \in \mathbb{Z}\}$ as a pair of low-pass and high-pass filters and $c_{j+1}[i]$ as the input signal, Equation 9 is implemented as Fig. 2 which is the famous Mallat algorithm [22].

C. Empirical wavelet transformation

The EWT is an automatic signal processing approach with solid theories in decomposing non-stationary time series [23]. Unlike DWT and EMD [24], EWT precisely investigates the time series

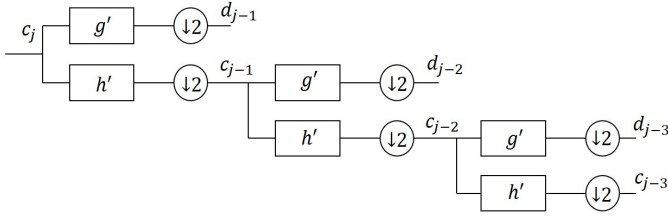


Fig. 2. Decomposition of Mallat algorithm

in the Fourier domain after fast Fourier transform (FFT). The EWT separates the spectrum using data-driven band-pass filtering.

In the EWT, limited freedom is provided for selecting wavelets. The algorithm employs Littlewood-Paley and Meyer's wavelets because of the analytic accessibility of the Fourier domain's closed-form formulations [25]. These band-pass filters' formulations are denoted using Equations 10 and 11

$$\hat{\phi}_n(\omega) = \begin{cases} 1 & \text{if } |\omega| \leq (1 - \gamma)\omega_n \\ \cos \left[\frac{\pi}{2} \beta \left(\frac{1}{2\gamma\omega_n} (|\omega| - (1 - \gamma)\omega_n) \right) \right] & \text{if } (1 - \gamma)\omega_n \leq |\omega| \leq (1 + \gamma)\omega_n \\ 0 & \text{otherwise,} \end{cases} \quad (10)$$

$$\hat{\psi}_n(\omega) = \begin{cases} 1 & \text{if } (1 + \gamma)\omega_n \leq |\omega| \leq (1 - \gamma)\omega_{n+1} \\ \cos \left[\frac{\pi}{2} \zeta \left(\frac{1}{2\gamma\omega_{n+1}} (|\omega| - (1 - \gamma)\omega_{n+1}) \right) \right] & \text{if } (1 - \gamma)\omega_{n+1} \leq |\omega| \leq (1 + \gamma)\omega_{n+1} \\ \sin \left[\frac{\pi}{2} \zeta \left(\frac{1}{2\gamma\omega_n} (|\omega| - (1 - \gamma)\omega_n) \right) \right] & \text{if } (1 - \gamma)\omega_n \leq |\omega| \leq (1 + \gamma)\omega_n \\ 0 & \text{otherwise,} \end{cases} \quad (11)$$

with a transitional band width parameter γ satisfying $\gamma \leq \min_n \frac{\omega_{n+1} - \omega_n}{\omega_{n+1} + \omega_n}$. The most common function $\zeta(x)$ in Equation 10 and 11 is presented in Equation 12. This empowers the formulated empirical scaling and wavelet function $\{\hat{\phi}_1(\omega), \{\hat{\psi}_n(\omega)\}_{n=1}^N\}$ to be a tight frame of $L^2(\mathbb{R})$ [26].

$$\beta(x) = x^4(35 - 84x + 70x^2 - 20x^3) \quad (12)$$

It can be observed that $\{\hat{\phi}_1(\omega), \{\hat{\psi}_n(\omega)\}_{n=1}^N\}$ are used as band-pass filters centered at assorted center frequencies.

D. Variational mode decomposition

VMD can decompose the non-stationary signals into several sub-series called modes [27]. The VMD can be considered as the following problem

$$\min \{m_k\}, \{w_k\} \left\{ \sum_{k=1}^K \|\delta_t \left[(\delta(t) + \frac{k}{\pi t}) \times m_j(t) \right] e^{k\omega_k t} \|_2^2 \right\} \quad (13)$$

with the constraints as

$$\sum_{k=1}^K m_k = x(t), \quad (14)$$

where m_k is mode k , ω_k is m_k 's central frequency, K is the number of modes, $x(t)$ represents the input time series. The problem shown in Equation 13 is transformed into Equation 15 when introducing the

L_2 penalty and Lagrange multiplier

$$L(\{m_k\}, \{w_k\}, \lambda) = \alpha \left\{ \sum_{k=1}^K \|\delta_t \left[(\delta(t) + \frac{k}{\pi t}) \times m_j(t) \right] e^{k\omega_k t} \|_2^2 + \right. \\ \left. \|x(t) - \sum_{k=1}^K m_k\| \left\langle \lambda(t), x(t) - \sum_{k=1}^K m_k \right\rangle \right\}. \quad (15)$$

The alternating direction method of multipliers (ADMM) algorithm is utilized to solve the above problem in VMD. Then the modes m_k and ω_k are obtained during the shifting process. According to the ADMM algorithm, the m_k and ω_k can be computed from the following equations,

$$\hat{m}_k^{n+1} = \frac{\hat{y}(\omega) - \sum_{i \neq k} \hat{m}_k(\omega) + \frac{\hat{\lambda}(\omega)}{2}}{1 + 2\alpha(\omega - \omega_k)^2} \quad (16)$$

$$\hat{\omega}_k^{n+1} = \frac{\int_0^\infty \omega |\hat{m}_j(\omega)|^2 d\omega}{\int_0^\infty |\hat{m}_j(\omega)|^2 d\omega}, \quad (17)$$

where n represents the number of iterations, $\hat{y}(\omega)$, $\hat{m}_k(\omega)$, $\hat{\lambda}(\omega)$ and \hat{m}_k^{n+1} represent the Fourier transform of $x(t)$, $m_j(t)$, $\lambda(t)$ and m_k^{n+1} , respectively.

This work uses "components" to represent sub-bands signals in EWT and DWT and IMFs in EMD and VMD. The input EEG signals are first decomposed into a pre-defined number of components channel-wise.

III. DECOMPOSITION-BASED HYBRID ENSEMBLE CNN FRAMEWORK

To better extract useful information from the decomposed components, end-to-end CNNs are employed to learn the components in our framework. Afterward, we propose a novel ensemble architecture for these CNN models corresponding to individual components. In this section, the ensemble learning method is presented. The structure of the overall framework is shown in Fig. 1.

A. Ensemble learning

In the framework, the number of branches is the same as the number of the decomposed components. That is to say, each component's data is inputted into the same CNN model. We employ two ensemble ways to integrate the model outputs. After decomposition, given label data \mathbf{y} , two ensemble modes are described as follows,

- 1) Train CNNs together (TT). For each individual CNN, we denote the obtained score before the Softmax layer of each model as $\{\mathbf{S}_a\}_{a \in [0, z]}$, where a is the index of the model, and $z = \text{the number of components}$. In each epoch, the scores of branches are averaged for each sample in the mini-batch, which can be formulated as

$$\mathbf{S}_o = \frac{1}{i} \sum_{a=0}^{a=z} \mathbf{S}_a, \quad (18)$$

where \mathbf{S}_o is the integrated output score before the Softmax layer. After passing the output score through the Softmax layer, the cross-entropy loss is computed, which is presented as

$$CE_Loss = - \sum \mathbf{y} \log(\mathbf{p}(\mathbf{S}_o)), \quad (19)$$

where $\mathbf{p}(\cdot)$ is the probability output of the Softmax layer. In overall, all CNNs in the ensemble structure are trained together.

- 2) Output fusion (OF). In this mode, at first, each CNN models corresponding to decomposed components are fully trained,

respectively. During testing, the outputs after the Softmax layer of the models are fused by averaging, which is presented as

$$p(S_0) = \frac{1}{z} \sum_{a=0}^{a=z} p(S_a). \quad (20)$$

Different from TT ensemble way, OF only trains z models simultaneously during training, and fuse the outputs of the Softmax layer. Since the model trained with less information correlated with the label has a low confidence level of classification output, the high confidence level output can contribute more to the results and correct the wrong classifications from low-level confidence models. Moreover, although some outputs are not high-level confidence, these models still capture useful information and contribute to the enhancement of the final accuracy to some extent. Therefore, any components should not be dropped during training.

B. component-specific batch normalization layer

Subject-variability problem limits the generalization ability of the obtained CNN models. Adaptive batch normalization (AdaBN) that was proposed by Li *et al.* has shown its superiority in reducing subject-variability [28]. AdaBN is that the mean and standard deviation (std) of batch normalization layer only use the statistics of the corresponding source domain or target domain, namely, training subjects data or testing subjects data. In our framework, we extend this setting to the models trained with decomposed components, and a component-specific batch normalization (CSBN) layer is used in our framework. Results in Section IV present that this CSBN setting improves the generalization ability of the trained ensemble model to the unseen subject's data.

IV. EXPERIMENTS

A. Introduction of Taiwan driving dataset

The pre-processed Taiwan driving dataset [29] is used in our study. In the experiment, lane-departure events were randomly induced to make the car drift from the original cruising lane towards the left or right sides (deviation onset). Each participant was instructed to quickly compensate for this perturbation by steering the wheel (response onset) to cause the car to move back to the original cruising lane (response offset). A complete trial included deviation onset, response onset, and response offset events.

In our study, fatigue-related SA is analyzed. We extracted three seconds of EEG data prior to the deviation onset. Then, we followed [28] to use local reaction time (RT) and global RT to label data. When both the local and global RT was shorter than 1.5 times the alert-RT, the corresponding extracted EEG data was labeled as "high SA." When both the local and global RT was longer than 2.5 times the alert-RT, the data was labeled as "low SA." Transitional states with moderate performance were excluded, and the neutral state was not considered in this work. For the subjects with multiple datasets, we selected the most balanced one to perform the filter operation. Then, we further down-sampled the data to 128Hz. Finally, we obtained a balanced SA dataset which included 2022 samples data of 11 subjects. The data size of one sample is 30 (channels) \times 384 (sample points).

B. Cross-subject situation awareness recognition results

1) **Experiment Settings:** The experiment was conducted on an Alienware Desktop with a 64-bit Windows 10 operation system powered by Intel(R) Core(TM) i7-6700 CPU and an NVIDIA GeForce GTX 1080 graphics card. The codes were implemented and tested

on the platform of Python 3.7.0. Pytorch framework was employed in this work.

In the proposed decomposition-based hybrid ensemble CNN framework, we adopted InterpretableCNN [16] as the backbone network. For convenience, we denoted the InterpretableCNN as ICNN and ensemble InterpretableCNN as EICNN. Considering the high complexity of EEG signals, we first set the number of decomposed components as 10. The specific sensitive test of the number of components will be described in section IV-C. After the decomposition for all channels, the lowest number of components obtained was 4 and 5 for EMD and DWT, respectively. Thus, these two parameters were adopted for subsequent tests. We proposed eight models under our framework by combining four decomposition methods and two ensemble methods. Our models are compared with strong baselines for cross-subject EEG-based recognition, including 1) power spectral density (PSD) features and support vector machine (SVM) classifier. Specifically, the PSD features in the frequency bands of alpha (8-12 Hz), theta (4-7 Hz), and delta (1-3 Hz) were utilized. 2) EEGNet-8,2 [15], 3) ConvNet [11], 4) InterpretableCNN [16] and 5) subject-matching model [28] which is a type of domain generalization framework to reduce the subject-variability problem by exploiting the similarity between subjects data.

The leave-one-subject-out cross-validation was conducted to evaluate the performance of the proposed framework. Regarding the hyper-parameter setting, we used Adam optimizer with momentum $\beta_1 = 0.9$, $\beta_2 = 0.99$. The mini-batch was 50, and the learning rate was 0.001. The model was trained for 50 epochs. We employed cross-entropy as the cost function for training. The hyper-parameters were the same for all the evaluated CNN models.

2) **Comparison results:** The mean cross-subject recognition performance was compared in Table II. We can observe that the proposed eight models under the framework all outperform the SOTA results and improve from 0.15% to 3.76%. In particular, DWT-based ensemble CNN with OF mode achieved new SOTA 82.11% accuracy. Better performance of the proposed models demonstrated the effectiveness of our framework. Moreover, we can observe that except for subject 7, other subjects' data results all outperformed the SOTA. In particular, the results of subjects 2 and 10 only attained lower than 70% by baseline methods. Contrastively, the performance of our models can be enhanced to even around 80%, resulting from the collaborative effect of each element in the framework.

We further investigated different elements in the framework. 1) **Ensemble ways:** The comparison of OF and TT modes for each of the decomposition methods were presented in Table II. Overall, OF outperformed TT. Specifically, except for the comparable results obtained by VMD, the OF results of other decomposition methods gained around 1% to 2% enhancement. 2) **Decomposition methods:** With the same parameter of 10 decomposed components for VMD and EWT, the ensemble model with EWT presented better results. In particular, the EWT-based model increased 2.04% compared with that of VMD in the OF ensemble mode. For EMD and DWT, since the signals were decomposed into the simplest IMFs, the model can capture primary features more easily. The better results of EMD and DWT presented in the table demonstrated this conclusion as well. 3) **CSBN:** To better analyze the effect of the CSBN layer in the framework, we added AdaBN in InterpretableCNN. In the Table II, **w** and **w/o** represented "with" and "without", respectively. Without CSBN, VMD- and EWT-based models both showed better accuracy compared with that of InterpretableCNN without AdaBN as well. Moreover, EMD- and DWT-based methods consistently presented a superior performance in the condition of with or without CSBN. It was observed that CSBN could bring stable improvement on the performance by approximately 3%. Compared with the improvement

of adding AdaBN on InterpretableCNN models by only around 2%, CSBN in the ensemble CNN model can better reduce the subject-variability. In addition, compared with the domain generalization algorithm [28], our model can extract better invariant features and achieve better cross-subject recognition performance. In the following sections, if there is no specification, the models with the CSBN layer are used to discuss the results.

To demonstrate the superiority of our proposed models, we first performed Friedman and Nemenyi post hoc test. Based on the critical distance (CD) 5.11, the results were shown in Fig. 3. We can conclude that the proposed models had the highest ranking. Then, in order to compare the proposed models with other models in a pair-wise fashion, the one-tail Wilcoxon paired signed-rank test was conducted. The p -values were shown in Table III. In the comparison inside the proposed models, only the significant p -values were listed. For convenience, we denoted decomposition-based EICNN (TT) as decomposition (TT) only in this table. The DWT-based and EMD-based TT models can beat all baseline models from the table. Other proposed models showed significant improvements over most baselines. On the other hand, in the internal comparison, the DWT-based OF model still showed a stronger capability of recognition that can beat almost all other decomposition methods- and TT-based models.

Friedman p-value: 1.86e-05 – CD: 5.11

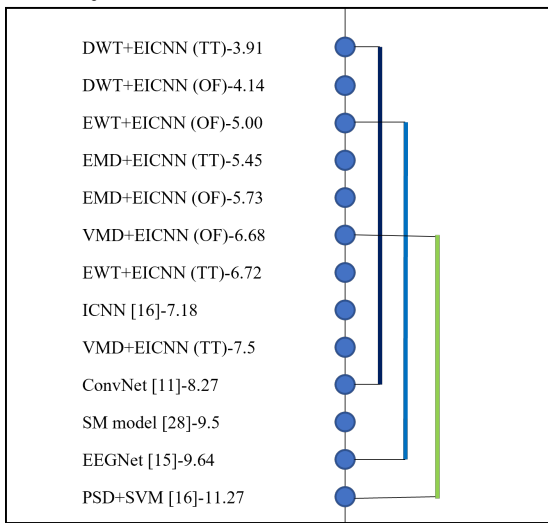


Fig. 3. Nemenyi test results

C. Ablation study

1) *Comparison between decomposition methods*: Since the higher-level decomposed components contain more complex information or more high-frequency noise, we investigated the impact of only using the first n components to the ensemble. The results were drawn in Fig. 4. It was observed that all models suffered from the negative impact of high-level components to a different extent. Specifically, DWT- and EMD-based models showed above 3% better performance when more than two components were used. Compared with the other three methods, the VMD-based model did not present a competitive performance at all points. Interestingly, although the DWT-based model achieved 82.65% at the peak of using the first four components, there was a decrease after four components, resulting from a large amount of high-frequency noise in the fifth and sixth components.

Then we studied the sensitivity of the number of decomposed components. The averaged accuracies on 11 subjects' data were

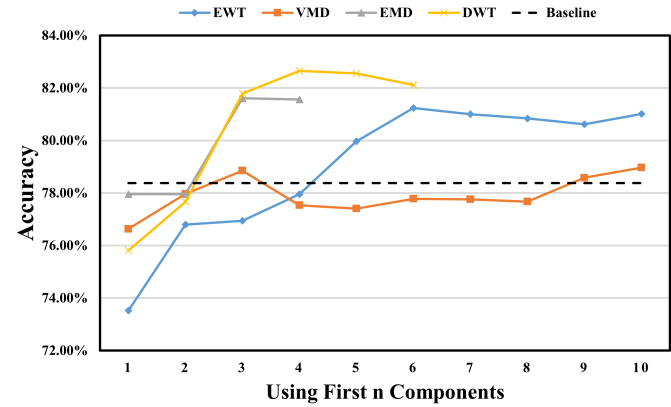


Fig. 4. Performance of using first n components

listed in Table I. For EMD and DWT, since the maximum number of decomposed components was four and six for each, the number smaller than this maximum was investigated. Overall, VMD- and DWT-based models trained with five components showed better performance among the compared component numbers. For EMD and EWT, the results of using four and ten components were better.

TABLE I
SENSITIVE TEST ON THE NUMBER OF DECOMPOSED COMPONENTS (%)

Methods	Number of components		
	3	5	7
VMD	79.28	80.92	79.36
EWT	79.47	79.59	80.38
EMD	80.66		
DWT	81.32	82.15	

2) *Investigation on different backbone networks*: Against the selection of the DNN model part in the framework, we investigated the impact of different CNN models. Specifically, we employed a ShallowCNN [30] and a deeper EEGNet, including two and three convolution layers, respectively. Since the original version of ShallowCNN does not include batch normalization (BN) layers, we adopted a variant with BN applied on the activations of the spatial convolutional layer. The results were shown in Table IV. We denoted ensemble EEGNet as EEEGNet and ensemble ShallowCNN as EShallowCNN. The ensemble EEGNet model showed better performance from the table than the SOTA InterpretableCNN, which demonstrated that the deeper CNN is more proper in our framework.

V. DISCUSSION

Our models with two ensemble modes achieved new SOTA performance based on the experiments. This section discusses the specific impact of the models with two types of ensemble modes on EEG data learning.

The same CNNs corresponding to the number of components is combined as a new ensemble model regarding the TT ensemble mode. The validation losses of 11 subjects in each fold were plotted in Fig. A1. In general, in 50 epochs, training loss for each subject can all be minimized to around 0.1, and the validation loss can attend to a minimum point except subject 7 data as the validation set. For subject 7, the validation loss starts from a minimum point and increases to approximately 1.5, resulting in the poor accuracy of classifying subject 7 data. Although this ensemble model can reduce the complexity and improve generalization ability overall, subject 7 data is still hard to classify samples. On the other hand, apart from

TABLE II
COMPARISON BETWEEN DECOMPOSITION-BASED HYBRID ENSEMBLE CNN FRAMEWORK AND SOTA METHODS (%)

Methods	Subjects											Mean
	1	2	3	4	5	6	7	8	9	10	11	
PSD+SVM [16]	77.66	75.76	66.67	66.22	83.04	75.90	59.80	67.80	88.54	70.37	59.73	71.95
EEGNet 8.2 [15]	76.06	66.67	61.33	81.76	78.13	75.90	66.67	75.38	78.66	85.19	69.47	74.11
ConvNet [11]	66.49	45.45	77.33	70.95	86.16	83.73	70.59	81.44	81.21	75.93	75.66	74.09
SM model [28]	78.72	68.18	79.33	68.24	85.27	83.73	64.71	57.2	78.03	82.41	71.68	74.32
ICNN [16]	w/o AdaBN	87.23	61.36	66.00	75.00	80.36	82.53	65.69	79.55	90.45	82.41	66.81
	w AdaBN	85.00	67.65	81.80	78.99	88.35	83.92	67.06	79.05	89.17	71.02	69.82
VMD+EICNN(TT)	w/o CSBN	89.36	60.61	71.33	69.59	75.45	86.14	68.63	72.35	86.94	84.26	72.57
	w CSBN	89.89	78.03	75.33	71.62	86.61	84.34	68.63	74.62	87.26	75.93	71.24
EWT+EICNN(TT)	w/o CSBN	88.30	67.42	76.67	71.62	79.02	77.71	69.61	70.83	87.90	82.41	68.58
	w CSBN	88.83	80.30	77.33	77.03	88.84	80.12	68.63	71.21	88.85	77.78	71.68
EMD+EICNN(TT)	w/o CSBN	89.36	59.09	82.00	77.03	78.13	83.13	65.69	75.38	87.58	80.56	69.47
	w CSBN	89.89	72.73	81.33	80.41	87.95	84.34	67.65	77.27	89.17	80.56	71.68
DWT+EICNN(TT)	w/o CSBN	89.36	62.12	82.00	78.38	83.04	87.35	63.73	79.55	89.17	82.41	80.09
	w CSBN	88.83	73.48	82.67	81.08	91.96	86.14	67.65	80.30	89.17	76.85	79.20
VMD+EICNN(OF)	w/o CSBN	89.89	65.15	74.67	68.24	83.93	83.73	70.59	76.52	87.90	81.48	76.11
	w CSBN	89.89	75.76	71.33	71.62	86.61	83.73	67.65	75.00	88.54	83.33	75.22
EWT+EICNN(OF)	w/o CSBN	88.83	68.94	78.67	72.30	81.25	81.93	68.63	75.38	90.45	79.63	74.34
	w CSBN	88.30	81.82	77.33	79.05	89.29	84.94	66.67	77.27	89.81	79.63	76.99
EMD+EICNN(OF)	w/o CSBN	89.36	68.94	78.00	71.62	81.25	84.94	67.65	76.89	88.22	77.78	73.89
	w CSBN	91.49	87.88	80.00	75.68	89.29	81.93	62.75	81.06	87.58	81.48	74.34
DWT+EICNN(OF)	w/o CSBN	89.36	63.64	82.00	79.05	87.95	88.55	56.86	82.20	90.13	81.48	76.99
	w CSBN	88.30	73.48	83.33	82.43	90.63	90.96	64.71	81.44	88.54	81.48	77.88
												82.11

TABLE III
WILCOXON RESULTS

	PSD+SVM	EEGNet 8.2	DeepNN	SM model	ICNN	VMD (TT)	EWT (TT)	EMD (TT)	Vmd (TT)
VMD+EICNN(TT)	0.0010	0.0737	0.3232	0.0508	0.5508				
EWT+EICNN(TT)	0.0005	0.0508	0.1931	0.0297	0.4155				
EMD+EICNN(TT)	0.0015	0.0093	0.0415	0.0047	0.0372				
DWT+EICNN(TT)	0.0015	0.0068	0.0068	0.0049	0.0025	0.0269			
VMD+EICNN(OF)	0.0038	0.0508	0.1206	0.0183	0.4492				
EWT+EICNN(OF)	0.0005	0.0109	0.0463	0.0093	0.0737	0.0049	0.0234		0.0415
EMD+EICNN(OF)	0.0010	0.0161	0.0615	0.0161	0.1826	0.0337	0.0508		
DWT+EICNN(OF)	0.0035	0.0049	0.0083	0.0035	0.0049	0.0210		0.0415	0.0463

TABLE IV
DIFFERENT BACKBONE NETWORKS IN FRAMEWORK (%)

Model	Subjects											Mean
	1	2	3	4	5	6	7	8	9	10	11	
VMD+EShallowCNN(OF)	82.98	44.70	72.00	79.05	83.93	89.76	68.63	72.35	90.13	78.70	83.19	76.86
EWT+EShallowCNN(OF)	84.57	80.30	74.67	70.27	88.84	83.73	66.67	75.76	90.13	75.00	79.20	79.01
EMD+EShallowCNN(OF)	76.06	53.79	80.00	79.05	87.95	85.54	67.65	78.03	87.90	82.41	78.32	77.88
DWT+EShallowCNN(OF)	86.70	57.58	83.33	85.14	90.18	88.55	70.59	84.09	86.94	78.70	81.42	81.20
VMD+EEEGNet(OF)	90.43	71.97	72.00	74.32	88.39	84.34	69.61	72.35	87.26	86.11	75.22	79.27
EWT+EEEGNet(OF)	88.30	80.30	78.67	79.05	87.95	88.55	63.73	73.86	89.17	81.48	79.65	80.97
EMD+EEEGNet(OF)	90.96	84.85	81.33	78.38	91.07	92.17	68.63	77.65	90.13	79.63	73.89	82.61
DWT+EEEGNet(OF)	89.36	72.73	83.33	80.41	94.20	95.78	68.63	83.33	87.58	83.33	79.65	83.48

TABLE V
THE PERFORMANCE ON EACH COMPONENT BY USING OF MODE (%)

Component	Subjects											Mean
	1	2	3	4	5	6	7	8	9	10	11	
1	85.11	81.06	76.00	66.89	78.57	86.14	58.82	71.21	80.89	73.15	76.11	75.81
2	87.23	86.36	80.00	72.30	78.13	85.54	61.76	71.97	84.08	70.37	74.78	77.50
3	81.91	84.85	76.67	83.78	87.50	90.36	66.67	82.20	89.17	79.63	73.45	81.47
4	82.45	68.94	77.33	78.38	88.39	87.35	69.61	81.44	85.03	85.19	69.91	79.46
5	87.23	69.70	79.33	74.32	87.50	89.76	68.63	73.86	82.80	77.78	78.32	79.02
6	89.36	59.09	83.33	81.08	89.29	85.54	69.61	77.65	88.85	79.63	76.11	79.96

the subject 1, 5, and 8 data of which the losses were significantly reduced, other subjects' data was generalized from the corresponding training set to some extent, which demonstrated the effectiveness of our new ensemble model.

Then we investigated the impact of the model in OF mode. The recognition accuracies by using each component were shown in Table V. We mainly analyzed the model of DWT-based ensemble InterpretableCNN with OF mode. We can observe that different components achieved the best results for each subject. The third component in DWT played an essential role for subjects 4, 5, 8, and 9, resulting in the better-averaged result of 81.47%. Compared with the result after the ensemble, 82.11%, our ensemble model exploited all components information and attained a better performance. There is a disadvantage along with using all components. After the ensemble, the lower results were usually observed for each subject. Therefore, during ensemble, how to reduce the impact of noise still requires to be further investigated.

VI. CONCLUSION

Against the challenge of EEG signals' non-stationary and complex problems, we propose a decomposition-based hybrid ensemble CNN framework that can easily capture more primary features from the simpler decomposed components. Moreover, a CSBN layer is added for each model in the framework. The proposed models under our framework showed superior performance than the SOTA results on the challenging leave-one-subject-out cross-validation SA recognition task. In particular, DWT-based ensemble EEGNet achieved the new SOTA, 83.48% mean accuracy. We further investigate the impact of decomposition methods. Results demonstrated that DWT-based models consistently improved over the baselines and other proposed models. In addition, the backbone model selection study indicated that deep CNNs in this ensemble structure have a more substantial capability to learn from the decomposed components. In conclusion, our proposed framework can significantly improve the EEG-based recognition performance. Regarding future work, since we observed that some high-level components harm the results because of the noise, the combination of component selection algorithms and the elimination of noises will be investigated.

REFERENCES

- [1] W. Dang, Z. Gao, D. Lv, X. Sun, and C. Cheng, "Rhythm-dependent multilayer brain network for the detection of driving fatigue," *IEEE Journal of Biomedical and Health Informatics*, vol. 25, no. 3, pp. 693–700, 2020.
- [2] Z. Lan, O. Sourina, L. Wang, R. Scherer, and G. R. Müller-Putz, "Domain adaptation techniques for eeg-based emotion recognition: a comparative study on two public datasets," *IEEE Transactions on Cognitive and Developmental Systems*, vol. 11, no. 1, pp. 85–94, 2018.
- [3] X. Yu, M. Z. Aziz, M. T. Sadiq, K. Jia, Z. Fan, and G. Xiao, "Computerized multidomain eeg classification system: A new paradigm," *IEEE Journal of Biomedical and Health Informatics*, 2022.
- [4] A. Anuragi, D. S. Sisodia, and R. B. Pachori, "Epileptic-seizure classification using phase-space representation of fbse-ewt based eeg subband signals and ensemble learners," *Biomedical Signal Processing and Control*, vol. 71, p. 103138, 2022.
- [5] N. Sairamya, M. Subathra, and S. T. George, "Automatic identification of schizophrenia using eeg signals based on discrete wavelet transform and rldip technique with ann," *Expert Systems with Applications*, vol. 192, p. 116230, 2022.
- [6] Y. Gu, X. Li, S. Chen, and X. Li, "Aoar: an automatic ocular artifact removal approach for multi-channel electroencephalogram data based on non-negative matrix factorization and empirical mode decomposition," *Journal of Neural Engineering*, vol. 18, no. 5, p. 056012, 2021.
- [7] V. P. Yadav and K. K. Sharma, "Variational mode decomposition-based seizure classification using bayesian regularized shallow neural network," *Biocybernetics and Biomedical Engineering*, vol. 41, no. 2, pp. 402–418, 2021.
- [8] M. T. Sadiq, X. Yu, and Z. Yuan, "Exploiting dimensionality reduction and neural network techniques for the development of expert brain-computer interfaces," *Expert Systems with Applications*, vol. 164, p. 114031, 2021.
- [9] I. Aliyu and C. G. Lim, "Selection of optimal wavelet features for epileptic eeg signal classification with lstm," *Neural Computing and Applications*, pp. 1–21, 2021.
- [10] P. Wang, M. Wang, Y. Zhou, Z. Xu, and D. Zhang, "Multiband decomposition and spectral discriminative analysis for motor imagery bci via deep neural network," *Frontiers of Computer Science*, vol. 16, no. 5, pp. 1–13, 2022.
- [11] R. T. Schirrmeister, J. T. Springenberg, L. D. J. Fiederer, M. Glasstetter, K. Eggensperger, M. Tangermann, F. Hutter, W. Burgard, and T. Ball, "Deep learning with convolutional neural networks for eeg decoding and visualization," *Human brain mapping*, vol. 38, no. 11, pp. 5391–5420, 2017.
- [12] P. Bashivan, I. Rish, M. Yeasin, and N. Codella, "Learning representations from eeg with deep recurrent-convolutional neural networks," *arXiv preprint arXiv:1511.06448*, 2015.
- [13] S. Sakhavi, C. Guan, and S. Yan, "Parallel convolutional-linear neural network for motor imagery classification," in *2015 23rd European Signal Processing Conference (EUSIPCO)*. IEEE, 2015, pp. 2736–2740.
- [14] Z. Yin and J. Zhang, "Cross-session classification of mental workload levels using eeg and an adaptive deep learning model," *Biomedical Signal Processing and Control*, vol. 33, pp. 30–47, 2017.
- [15] V. J. Lawhern, A. J. Solon, N. R. Waytowich, S. M. Gordon, C. P. Hung, and B. J. Lance, "Eegnet: a compact convolutional neural network for eeg-based brain-computer interfaces," *Journal of neural engineering*, vol. 15, no. 5, p. 056013, 2018.
- [16] J. Cui, Z. Lan, O. Sourina, and W. Müller-Wittig, "Eeg-based cross-subject driver drowsiness recognition with an interpretable convolutional neural network," *IEEE Transactions on Neural Networks and Learning Systems*, pp. 1–13, 2022.
- [17] P. Wang, A. Jiang, X. Liu, J. Shang, and L. Zhang, "Lstm-based eeg classification in motor imagery tasks," *IEEE transactions on neural systems and rehabilitation engineering*, vol. 26, no. 11, pp. 2086–2095, 2018.
- [18] Y. Zhang, H. Cai, L. Nie, P. Xu, S. Zhao, and C. Guan, "An end-to-end 3d convolutional neural network for decoding attentive mental state," *Neural Networks*, vol. 144, pp. 129–137, 2021.
- [19] O. Sagi and L. Rokach, "Ensemble learning: A survey," *Wiley Interdisciplinary Reviews: Data Mining and Knowledge Discovery*, vol. 8, no. 4, p. e1249, 2018.
- [20] N. E. Huang, Z. Shen, S. R. Long, M. C. Wu, H. H. Shih, Q. Zheng, N.-C. Yen, C. C. Tung, and H. H. Liu, "The empirical mode decomposition and the hilbert spectrum for nonlinear and non-stationary time series analysis," *Proceedings of the Royal Society of London. Series A: mathematical, physical and engineering sciences*, vol. 454, no. 1971, pp. 903–995, 1998.
- [21] I. Daubechies, "Orthonormal bases of compactly supported wavelets," *Communications on Pure and Applied Mathematics*, vol. 41, no. 7, pp. 909–996, 1988.
- [22] S. G. Mallat, "A theory for multiresolution signal decomposition: the wavelet representation," *IEEE Transactions on Pattern Analysis and Machine Intelligence*, vol. 11, no. 7, pp. 674–693, 1989.
- [23] J. Gilles, "Empirical wavelet transform," *IEEE transactions on signal processing*, vol. 61, no. 16, pp. 3999–4010, 2013.
- [24] P. Flandrin, G. Rilling, and P. Goncalves, "Empirical mode decomposition as a filter bank," *IEEE signal processing letters*, vol. 11, no. 2, pp. 112–114, 2004.
- [25] J. Spencer, *Ten lectures on the probabilistic method*. SIAM, 1994, vol. 64.
- [26] P. G. Casazza *et al.*, "The art of frame theory," *Taiwanese Journal of Mathematics*, vol. 4, no. 2, pp. 129–201, 2000.
- [27] K. Dragomiretskiy and D. Zosso, "Variational mode decomposition," *IEEE transactions on signal processing*, vol. 62, no. 3, pp. 531–544, 2013.
- [28] R. Li, L. Wang, and O. Sourina, "Subject matching for cross-subject eeg-based recognition of driver states related to situation awareness," *Methods*, 2021.
- [29] Z. Cao, C.-H. Chuang, J.-K. King, and C.-T. Lin, "Multi-channel eeg recordings during a sustained-attention driving task," *Scientific data*, vol. 6, no. 1, pp. 1–8, 2019.
- [30] H. Dose, J. S. Møller, H. K. Iversen, and S. Puthusserpady, "An end-to-end deep learning approach to mi-eeg signal classification for bcis," *Expert Systems with Applications*, vol. 114, pp. 532–542, 2018.